

Exciton localization on p-i-n junctions in two-dimensional crystals

Bartłomiej Szafran

AGH University of Science and Technology,
Faculty of Physics and Applied Computer Science,
al. Mickiewicza 30, 30-059 Kraków, Poland

We consider a neutral exciton localized on a model p-i-n junction defined in a two-dimensional crystal: MoSe₂ and phosphorene, using a variational approach to the effective mass Hamiltonian. The variational solution to the problem with non-separable center of mass provides the exciton density in the real space and accounts for the kinetic energy due to the exciton localization. For low values of the potential step across the junction, the exciton occupies an area which is much larger than the nominal width of the junction. Localization of the exciton within the junction area is accompanied by the appearance of the dipole moment induced by the local electric field. The induced dipole moment becomes a linear function of the potential step only when the step is sufficiently large. In consequence, the energy dependence on the step value is non-parabolic. We demonstrate that the exciton gets localized not exactly at the center of the junction but on the side which is more energetically favourable for the heavier carrier: electron or hole.

I. INTRODUCTION

Reduction of dimensionality and large carrier effective masses in monolayer transition-metal dichalcogenide [1, 2] and phosphorene [3, 4] result in large exciton binding energies [5–12] exceeding by two orders of magnitude the corresponding values in bulk semiconductors. Large binding energy allows for tuning the exciton line in the luminescent spectrum by the Stark effect induced by an in-plane electric field [9] which leads to a red-shift of the electron-hole recombination energy due to the interaction of the intrinsic or induced exciton dipole moment with the field. The Stark effect was studied for states in quantum wells [13, 14] or quantum dots [15–18] where the quantum confinement stabilized the weakly bound exciton against dissociation by the electric field. Conversely, the Stark effect for strongly bound excitons in a transition metal dichalcogenide has recently been used to trap the excitons on the electric field at the p-i-n junction [19].

The purpose of the present work is to describe the exciton confinement in a model of the p-i-n junction by a numerical albeit exact solution of the two-particle problem. The trapping mechanism was explained [19] as due to an effective potential for the exciton that contains a term due to the electric field $V_{eff}(x) = -\frac{1}{2}\alpha_p|F_x(x)|^2$, where F_x is the electric field at the junction and α_p is the polarizability of the exciton, which for the homogeneous electric field can be determined by the solution of the electron-hole problem in the relative electron-hole coordinates [9, 10, 19]. The electric field in the junction [19] is not homogeneous and the motion of the center of mass of the exciton does not separate from the eigenproblem in the relative coordinates. Therefore, the center of mass requires treatment on equal rights with the relative electron-hole coordinates which we provide in this work. The solution accounts for the kinetic energy due to the exciton confinement at the junction and provides information on the exciton localization: its mean position and extent of its wave function in the real space. We find that the range of exciton confinement depends strongly on the

value of the potential step at the junction, and for a low value of the step the confinement range can largely exceed the nominal width of the junction. Then, the wave function is present in a region with a widely changing electric field that makes the homogeneous field solution not directly adequate to a local field case. In particular, the electric field at the center of the junction is a linear function of the potential step at the junction, but the induced dipole moment is not and the reaction of the exciton energy on the step is not parabolic as for Stark effect in the homogenous electric field.

II. THEORY

We work with the effective band Hamiltonian for the electron-hole pair at the junction

$$H = -\frac{\hbar^2}{2m_e^x} \frac{\partial^2}{\partial x_e^2} - \frac{\hbar^2}{2m_e^y} \frac{\partial^2}{\partial y_e^2} - \frac{\hbar^2}{2m_h^x} \frac{\partial^2}{\partial x_h^2} - \frac{\hbar^2}{2m_h^y} \frac{\partial^2}{\partial y_h^2} + V(x_e) - V(x_h) - V_{eh}(r_{eh}), \quad (1)$$

with $m_{e/h}^{y/x}$ standing for the electron or hole mass along the x or y directions. We use the model potential of the p-i-n junction in the form $V(x) = -e\frac{2V_0}{\pi} \arctan(\frac{x}{d})$ where V_0 defines the scale of the potential step along the junction and the variation rate is given by d . The model potential is plotted in Fig. 1 for the electron ($V(x)$, red line) and the hole ($-V(x)$, black line). The potential pushes the non-interacting carriers away from the junction center. In Eq. (1) $V_{eh}(r_{eh})$ is the effective 2D interaction given by the Keldysh potential [7–12, 19–22],

$$V_{eh}(r) = \frac{e^2}{4\pi\epsilon_0} \frac{\pi}{2\epsilon r_0} [H_0(r/r_0) - Y_0(r/r_0)], \quad (2)$$

where H_0 and Y_0 are the Struve and Bessel functions of the second kind, r_0 is the screening length that is a measure of the polarizability of the 2D semiconductor and ϵ is the dielectric constant. At large electron-hole distances $r \gg r_0$ the interaction potential tends to the

3D Coulomb form $1/r$. At small electron-hole distances $r \ll r_0$, V_{eh} acquires a logarithmic singularity of the 2D Coulomb potential. For evaluation of the interaction potential we use the method of Ref. [22]. The intrinsic area where the exciton confinement occurs in the experiment [19] has a length of several dozens of nanometers. Here we discuss the results with the parameter d ranging from 15 to 60nm. The variation of the potential by V_0 and $1.5V_0$ occurs at lengths of $2d$ and $2.4d$, respectively. In the experimental situation [19] the carriers are additionally confined by the space-charge density outside the intrinsic region. Here we assume that the depletion region is arbitrarily wide for a description of the exciton binding purely on the local electric field.

Using the center-of-mass coordinates $X = \frac{m_e^x x_e + m_h^x x_h}{M_x}$, $Y = \frac{m_e^y y_e + m_h^y y_h}{M_y}$, with $M_x = m_e^x + m_h^x$, $M_y = m_e^y + m_h^y$ and the relative electron-hole coordinates $x_{eh} = x_e - x_h$ and $y_{eh} = y_e - y_h$, the Hamiltonian is written as

$$H = -\frac{\hbar^2}{2M_x} \frac{\partial^2}{\partial X^2} - \frac{\hbar^2}{2M_y} \frac{\partial^2}{\partial Y^2} - \frac{\hbar^2}{2\mu_x} \frac{\partial^2}{\partial x_{eh}^2} - \frac{\hbar^2}{2\mu_y} \frac{\partial^2}{\partial y_{eh}^2} + V(x_e) - V(x_h) - V_{eh}(r_{eh}), \quad (3)$$

with the reduced masses $\mu_x = m_e^x m_h^x / (m_e^x + m_h^x)$ and $\mu_y = m_e^y m_h^y / (m_e^y + m_h^y)$. The motion of the center of mass along the junction separates from the rest of the coordinates, and we assume that the wave function over Y has the form of a plane wave with a zero wave vector. For a constant electric field oriented along the x direction, studied for the discussion of the Stark effect [9, 10, 19], the center of mass coordinate X also separates, but this is not the case for the present problem with the non-linear potential of the junction V .

The exciton states are determined using a variational approach [8] with Gaussian basis

$$\Phi(x_{eh}, y_{eh}, X) = \sum_{ijk} c_{ijk} \phi_{ijk}(x_{eh}, y_{eh}, X) = \quad (4)$$

$$\sum_{ijk} c_{ijk} \exp\left(-\frac{(x_{eh} - \kappa_i)^2}{\alpha} - \frac{(y_{eh} - \gamma_j)^2}{\beta} - \frac{(X - \eta_k)^2}{\gamma}\right),$$

where c_{ijk} are the linear variational coordinates determined by solving the generalized eigenvalue problem $\mathbf{Hc} = E\mathbf{Sc}$, with the matrix elements $H_{i'j'k',ijk} = \langle \phi_{i'j'k'} | H | \phi_{ijk} \rangle$ and $S_{i'j'k',ijk} = \langle \phi_{i'j'k'} | \phi_{ijk} \rangle$. The centers of the Gaussian are distributed on a 3D mesh with $\kappa_i = i\Delta_{x_{eh}}$, $\gamma_j = j\Delta_{y_{eh}}$ and $\eta_k = k\Delta_X$, with i, j and k being integers ranging from $-N$ to N . The values of Δ select the region in space to be described by the variational wave function. The spacings Δ 's and the localization parameters of the Gaussian α, β and γ are determined as nonlinear variational parameters by minimization of the energy estimate. Separate parameters for x_{eh} and y_{eh} are needed for phosphorene with its strongly anisotropic effective masses [23, 24] but also for the case of isotropic effective masses applied for MoSe₂ due to the external potential acting only in the x direction. The following results are obtained for $N = 8$, i.e. 17 Gaussians

describing the wave function in each coordinate, i.e. for the total number of $17^3 = 4913$ Gaussian functions used in the basis. The basis (4) is flexible enough to account for both the bound excitons and dissociated electron-hole pairs.

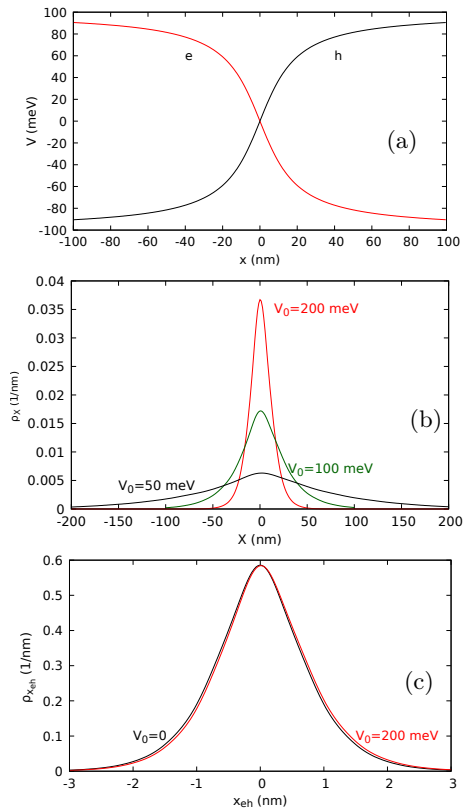


FIG. 1. (a) The model potential of the p-i-n junction $V(x) = -\frac{2eV_0}{\pi} \arctan(\frac{x}{d})$ for the electron (red curve) and $-V(x)$ potential for the hole (black curve) for $d = 15$ nm and $V_0 = 100$ meV. (b) The exciton density as a function of the center of mass position for $d = 15$ nm and three values of V_0 for the lowest-energy bound exciton state. (c) The probability density as a function of the electron-hole distance in the x direction x_{eh} for $V_0 = 0$ (black line) and $V_0 = 200$ meV (red line). MoSe₂ parameters are applied.

III. RESULTS AND DISCUSSION

A. MoSe₂

We first consider the material where the exciton trapping at the junction was accomplished [19], MoSe₂, the transition-metal dichalcogenide for which an isotropic effective mass model can be adopted with $m_e^x = m_e^y = 0.7m_0$ [19, 25] and $m_e^x = m_e^y = 0.6m_0$ [19, 26]. We take the dielectric constant $\epsilon = 4.4$ and the screening length $r_0 = 0.886$ nm after Ref. [19].

Figure 1(b) shows the lowest bound exciton state density calculated as $\rho_X(X) =$

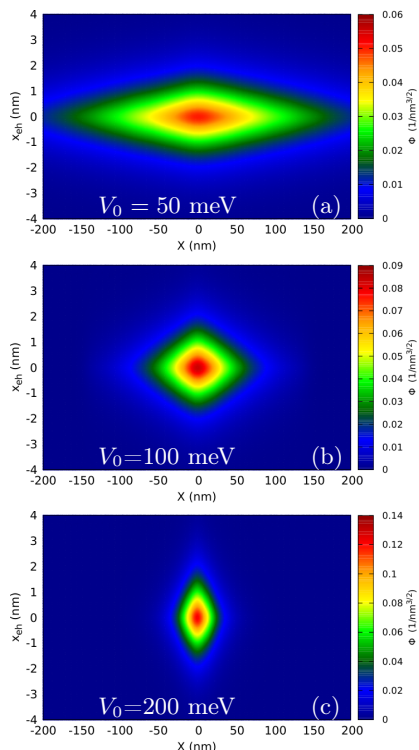


FIG. 2. Cross section of the lowest-energy bound wave function taken at $y_{eh} = 0$ $\Phi(x_{eh}, y_{eh} = 0, X)$ for $d = 15$ nm and MoSe₂ parameters.

$\int_{-\infty}^{\infty} dx_{eh} \int_{-\infty}^{\infty} dy_{eh} |\Phi(x_{eh}, y_{eh}, X)|^2$ for $d = 15$ nm. The exciton is localized near the area where the potential gradient is maximal, and the exciton localization increases with V_0 . The center of the exciton is localized off the center of the junction on the side of the junction where the heavier carrier – here the electron – has a lower potential energy (see below). Figure 1(c) shows the density over the horizontal electron-hole distance $\rho_{x_{eh}}(x_{eh}) = \int_{-\infty}^{\infty} dX \int_{-\infty}^{\infty} dy_{eh} |\Phi(x_{eh}, y_{eh}, X)|^2$. The potential of the considered range produces only a small shift of the density to a more positive x_{eh} , with the electron shifted to a more positive x and the hole to a more negative x position. The electron and hole densities calculated from the total wave function (not shown) are nearly identical to the exciton density ρ_X due to the large extent of ρ_X and the relative strong localization of the pair.

Figure 2 displays the cross section of the lowest energy bound electron-hole wave function taken at $y_{eh} = 0$ for $V_0 = 50$ meV, 100 meV and 200 meV. The range of the localization changes radically with V_0 only in the X coordinate and not in x_{eh} .

The process of exciton localization at the junction is illustrated in Fig. 3 where we considered several junction width parameters d . The energy decrease with V_0 in Fig. 3(a) is a signature of the carrier separation by the electric field which, as we find, does not start at zero V_0 (Fig. 3(a)). The exciton localization in the region of a large

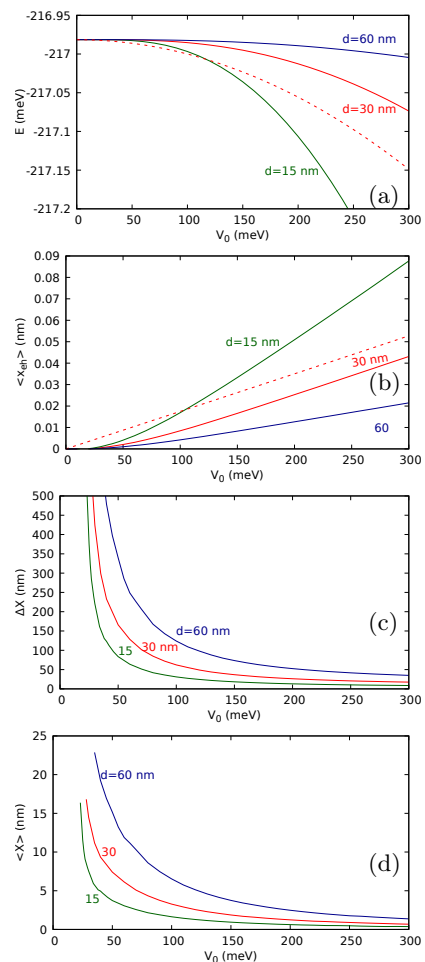


FIG. 3. (a) Energy of the lowest bound exciton state as a function of V_0 for varied values of the width of the junction d for MoSe₂. The dashed line shows the results for the junction potential replaced by its linear approximation $V_i(x) = -e \frac{2V_0}{\pi} \frac{x}{d}$ for $d = 30$ nm. (b) The average shift of the electron and hole position along the direction of the junction x_{eh} . The dashed line corresponds to the linear approximation as in (a). (c) The exciton localization width calculated from the wave function as $\Delta X = \langle (X - \langle X \rangle)^2 \rangle^{1/2}$. (d) The average position of the exciton center of mass. The line is plotted for V_0 where ΔX falls below 500 nm. The results correspond to the lowest-energy bound exciton state.

electric field is associated with the cost of additional kinetic energy. For larger values of d the electric field at the junction is lower, but the extent of exciton localization at the junction is decreased. The energy shift in the homogenous electric field falls with the square of the field [9, 10] which for the present potential implies a $-1/d^2$ dependence while the exciton confinement energy depends on the localization as $1/d^2$. The two effects seem to cancel each other out in the constant energy range of small V_0 . We observe that a nonzero value of the potential step is necessary to induce a significant dipole moment (Fig. 3(b)). As non-zero V_0 is introduced the range of exciton localization (Fig. 3(c)) becomes finite. However, for low

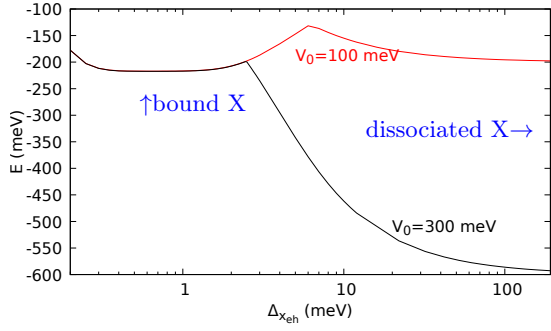


FIG. 4. The lowest energy estimate for $d = 15$ nm with $V_0 = 100$ meV (red line) and 300 meV (black line) for fixed $\Delta X = 18$ nm (see the description of the variational wave function given by Eq. (4)), as a function of Δx_{eh} . For this plot we keep $\Delta y_{eh} = \Delta x_{eh}$ and the Gaussian localization parameters $\alpha = \frac{\Delta x}{1.5}$, and $\beta = \gamma = \frac{\Delta x_{eh}^2}{1.5}$. The minimum near $\Delta x_{eh} = 0.8$ nm corresponds to the bound exciton. The results for large Δx_{eh} limit tend to $-2V_0$ and correspond to the dissociated exciton.

V_0 most of the exciton stays outside of the action range of the local electric field (potential gradient) at the junction. For all studied d values, the exciton size in terms of $\Delta X = \langle (X - \langle X \rangle)^2 \rangle^{1/2}$ becomes equal to double the width parameter $\Delta X = 2d$ for $V_0 \simeq 100$ meV. Only once the exciton is localized at the junction does the electron-hole system energy start to decrease visibly.

For comparison in Fig. 3(a) and (b) we plotted with the dashed red line the results for the homogenous electric field, i.e. for the potential of the junction replaced by its linear approximation: $V_l(x) = -e\frac{2V_0}{\pi}\frac{x}{d}$, for $d = 30$ nm. For $V_l(x)$ potential the dipole moment grows linearly with V_0 [Fig. 3(b)] starting from $V_0 = 0$. The linear dependence of the dipole moment via its interaction with the field produces the parabolic $E(V_0)$ dependence (the dashed line in Fig. 3(a)). For the junction potential $V(x)$, the growth of the dipole moment with V_0 follows after a delay. For all d considered the dipole moment starts to grow for $V_0 \gtrsim 20$ meV and becomes a linear function of V_0 only above $\simeq 100$ meV.

Figure 3(d) shows that the center of mass of the exciton approaches the center of the junction only in the $V_0 \rightarrow \infty$ limit, and for finite V_0 it stays on the positive side of the center of the junction. We return to this point for phosphorene, where the effect is more pronounced.

The ground-state energy $E_{gs}(0) = -216.89$ meV obtained at V_0 (Ref. [19] indicates -217 meV) implies that the dissociated electron-hole pair appears in the ground state for $V_0 \geq E_{gs}/2$. For $V_0/2$ above E_{gs} the bound hole-pair is not the ground state of the system, similarly to the studies of the Stark effect for a nonzero homogeneous electric field [9, 10, 19]. The applied basis resolves two separate minima for the bound and dissociated exciton. The results of the Hamiltonian diagonalization as a function of $\Delta x_{eh} = \Delta y_{eh}$ are given in Fig. 4, with the lower energy state corresponding to the bound exciton or the

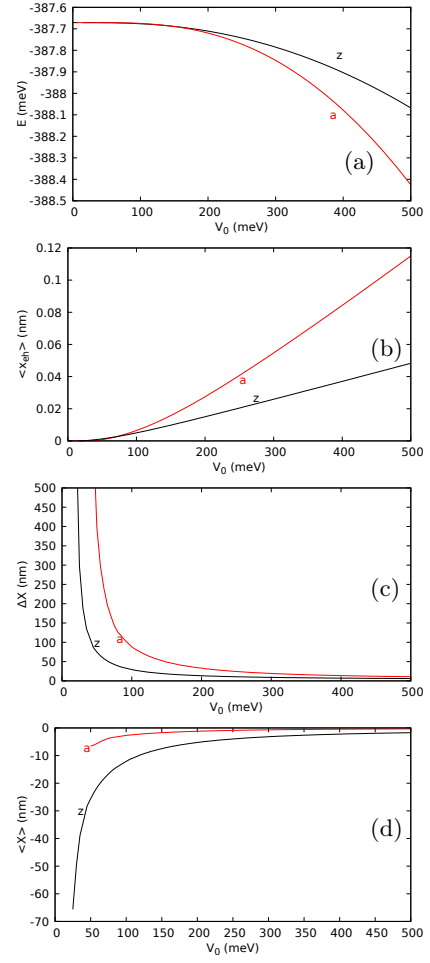


FIG. 5. (a) Energy of the lowest bound exciton state as a function of V_0 for monolayer phosphorene with the direction defining the p-i-n junction x aligned to the zigzag ('z', black line) or armchair ('a', red line) crystal direction (b) The average shift of the electron and hole position along the direction of the junction x_{eh} . (c) The exciton localization width ΔX . (d) The average position of the exciton center of mass.

dissociated pair for $V_0 = 100$ meV and 300 meV, respectively. Here, we discuss only the properties of the bound electron-hole state for both V_0 below or above the dissociation threshold. The gradient minimalization method applied for optimization of the non-linear variational parameters tends to the closest energy minimum, so one can choose between the dissociated or bound exciton states.

B. phosphorene

The effective masses in phosphorene exhibit strong anisotropy with larger (smaller) values in the zigzag (armchair) crystal direction [23, 24]. For monolayer black phosphorous, we adopted the values of effective masses derived by fitting the results of the single-band approximation to the results of the atomistic tight-binding [27]

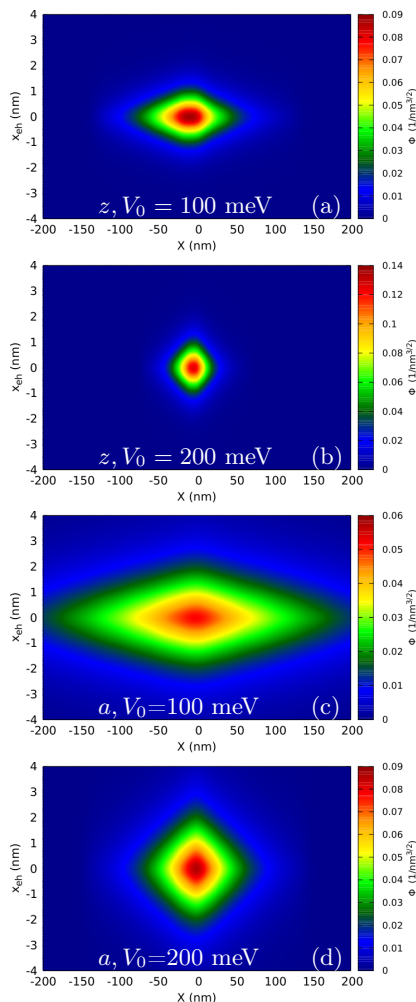


FIG. 6. Cross section of the wave function taken at $y_{eh} = 0$ $\Phi(x_{eh}, y_{eh} = 0, X)$ for $d = 15$ nm and phosphorene parameters. In (a) and (b) the p-i-n junction is defined along the zigzag crystal direction. Armchair direction is chosen in (c) and (d).

modelling for the harmonic oscillator confinement potential of Ref. [28]. That is, we take $m_a^e = 0.17037m_0$, $m_z^e = 0.85327m_0$ for the electron masses in the armchair and zigzag directions [28], respectively. For hole we take $m_a^h = 0.18972m_0$ for the armchair direction [28]. The hole mass in the zigzag direction was not adopted from Ref. [28] but set to $2.8m_0$. The literature values for the zigzag mass of the hole vary from $\simeq 1.13m_0$ [24, 29] to $\simeq 5$ [30] or $\simeq 6$ [31]. The selected choice of the effective masses provides the electron-hole pair reduced masses that agree with the ones given in Table 2 of Ref. [4] for monolayer phosphorene. For the interaction potential we take the screening length of $r_0 = 1.079$ nm and the effective dielectric constant of $\epsilon = 2.4$ after Supporting Information to Ref. [4].

In calculations for phosphorene we fix the junction width parameter to $d = 15$ nm. We keep the junction potential variation along the x axis that we align with ei-

ther armchair or zigzag crystal direction. The reaction of the exciton energy to the external potential is prompter for the junction defined along the armchair direction (Fig. 5(a)), and the induced dipole moment [Fig. 5(b)] is also larger in this direction where the masses are lighter. This finding is consistent with the conclusions of Ref. [9] for the case of a homogeneous electric field in phosphorene.

The cross sections of the wave function for $y_{eh} = 0$ is plotted in Fig. 6 for the zigzag (a,b) and armchair (c,d) orientation of the wave function. The orientation of the junction has a pronounced effect on the exciton localization along the X axis with the total mass $M_x = 0.36m_0$ for the armchair orientation $M_X = 3.65m_0$ for the junction defined along the zigzag crystal direction. The reduced mass in the x_{eh} direction is $0.089m_0$ for the armchair and $0.65m_0$ for the zigzag orientation, hence the varied localization along the vertical axis of Fig. 6. Fig. 5(c) indicates that the width of the exciton wave function becomes equal to $2d$ for $V_0 \simeq 100$ meV ($V_0 \simeq 210$ meV) for the junction defined along the zigzag (armchair) direction.

For phosphorene, the center of the exciton density is shifted to the left of the junction center [Fig. 6 and Fig. 5(d)]. The shift is smaller for the armchair orientation of the junction [Fig. 6(c,d)] and large for the zigzag-oriented junction [Fig. 6(a,b) and Fig. 5(d)]. As a general rule, the shift is large when one of the carriers is much heavier than the other and the shift appears in the direction of lower potential energy in the $V(x)$ potential for the heavier carrier. In the results for MoSe₂ (precedent subsection), the shift was observed to the positive side of the junction and the electron was slightly heavier. For phosphorene, the hole is heavier and the center of mass is shifted to the negative side of the junction. For the zigzag orientation, the mass difference is very pronounced; hence, the strong shift, much larger than the average electron-hole distance. The shift is directly related to the potential landscape at the junction. In Fig. 7 we plotted the external potential for both carriers, i.e. $V(x_e) - V(x_h)$ on the (X, x_{eh}) plane. The anisotropy of the masses translates to a shift of the potential minimum to the negative side of X , which produces the pronounced asymmetry for the zigzag orientation of the junction. The interaction potential of Hamiltonian (3) is independent of X and creates a valley along $x_{eh} = 0$ of depth that depends on y_{eh} . The displacement of the wave function to positive x_{eh} is not very pronounced (see Fig. 6 and Fig. 5(b)) since the strong interaction potential keeps the carriers close to one another. Instead, the wave function is shifted to the negative side of the junction where the minimum of the potential landscape is closer to the $x_{eh} = 0$ axis. The effect is particularly well seen in Fig. 6(a,b) (see also Fig. 5(d)). Note that for a homogeneous electric field, only the reduced masses and not the separate masses of the electron and hole matter for the properties of the bound exciton states [9].

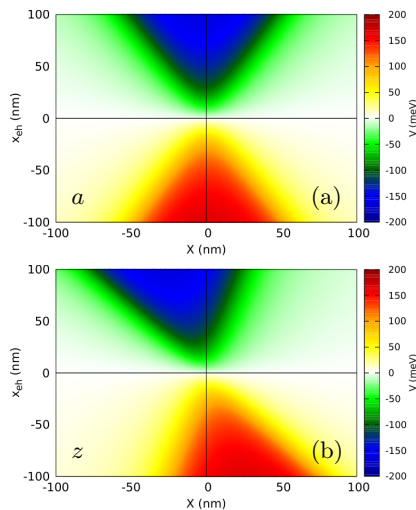


FIG. 7. Potential landscape $V(x_e) - V(x_h)$ at the junction for $d = 15$ nm, $V = 100$ meV for phosphorene parameters and the junction defined along the armchair (a) and zigzag (b) crystal direction.

IV. SUMMARY AND CONCLUSIONS

We have studied bound electron-hole pairs at a p-i-n junction defined within a two-dimensional crystal using a model with a finite spatial range and potential step V_0

across the junction with the electric field in the center of the junction proportional to V_0 . The problem was solved with a variational calculation using the basis of Gaussians centered on a grid spanned by the relative coordinates of the carriers and the center of mass, which is not separable in the inhomogeneous electric field. The appearance of the dipole moment induced by the local electric field at the junction is accompanied by a build-up of the exciton kinetic energy as a result of the localization at the junction. The compensation of the two contributions leads to a range of values of the potential step of the junction V_0 that has a negligible influence on the exciton energy. For MoSe₂ and phosphorene, localization of the exciton wave function in a range comparable with the junction length requires a potential difference across the junction of the order of $V_0 \simeq 100$ meV. For lower V_0 values, the carriers occupy the region in space where the electric field is much smaller than at the center of the junction. The induced dipole moment dependence on the potential step V_0 deviates from linear, which is expected for the Stark effect in a homogenous electric field. In consequence, the exciton energy is not a parabolic function of V_0 . We have demonstrated that the localized exciton is shifted off the center of the junction in the direction in which the junction potential energy for the heavier carrier is lower.

ACKNOWLEDGMENTS

Calculations for this work were performed on the PL-GRID infrastructure.

-
- [1] Q. H. Wang, K. Kalantar-Zadeh, A. Kis, J. N. Coleman, and M. S. Strano, *Nat. Nanotechnol.* **7**, 699 (2012).
 - [2] A. K. Geim and I. V. Grigorieva, *Nature (London)* **499**, 419 (2013).
 - [3] F. Xia, H. Wang, and Y. Jia, *Nat. Commun.* **5**, 4458 (2014).
 - [4] A.Castellanos-Gomez, L. Vicarelli, E. Prada, J.O. Island, K. L. Narasimha-Acharya, S. I Blanter, D. J. Groenendijk, M. Buscema, G.A. Steele, J. V. Alvarez, H. W. Zandbergen, J.J. Palacios, and H.S.J. van der Zant, *2D Materials* **1**, 025001 (2014).
 - [5] V. Tran, R. Soklaski, Y. Liand, and L. Yang, *Phys. Rev. B* **89**, 235319 (2014).
 - [6] L. Seixas, A. S. Rodin, A. Carvalho, and A. H. Castro Neto, *Phys. Rev. B* **91**, 115437 (2015).
 - [7] D.V. Tuan, M. Yang, and H. Dery, *Phys. Rev. B* **98**, 125308 (2018).
 - [8] D.W. Kidd, D.K. Zhang, and K. Varga, *Phys. Rev. B* **93**, 125423 (2016).
 - [9] A. Chaves, T.Low, P. Avouris, D. Cakir, and F.M. Peeters, *Phys. Rev. B* **91**, 155311 (2015).
 - [10] L. S. R. Cavalcante, D. R. da Costa, G. A. Farias, D. R. Reichman, and A. Chaves, *Phys. Rev. B* **98**, 245309 (2018).
 - [11] A.S. Rodin, A. Carvalho, and A.H. Castro Neto, *Phys. Rev. B* **90**, 075429 (2014).
 - [12] M. Van der Donck and F.M. Peeters, *Phys. Rev. B* **98**, 235401 (2018).
 - [13] D. A. B. Miller, D. S. Chemla, T. C. Damen, A. C. Gosard, W. Wiegmann, T. H. Wood, and C. A. Burrus *Phys. Rev. Lett.* **53**, 2173 (1984).
 - [14] Y.-H. Kuo, Y.K. Lee, Y. Ge, S. Ren, J. E. Roth, T.I. Kamins, D.A.B Miller, J.S. Harris, *Nature.* **437** 1334 (2005).
 - [15] P. W. Fry, I. E. Itskevich, D. J. Mowbray, M. S. Skolnick, J. J. Finley, J. A. Barker, E. P. O'Reilly, L. R. Wilson, I. A. Larkin, P. A. Maksym, M. Hopkinson, M. Al-Khafaji, J. P. R. David, A. G. Cullis, G. Hill, and J. C. Clark *Phys. Rev. Lett.* **84**, 733 (2000).
 - [16] W. Sheng and J.-P. Leburton, *Phys. Rev. Lett.* **88**, 167401 (2002).
 - [17] K. L. Janssens, B. Partoens, and F. M. Peeters, *Phys. Rev. B* **65**, 233301 (2002)
 - [18] H. J. Krenner, M. Sabathil, E. C. Clark, A. F. Kress, D. Schuh, M. Bichler, G. Abstreiter, and J. J. Finley, *Phys. Rev. Lett.* **94**, 057402 (2005).
 - [19] D. Thureja, A. Imamoglu, T. Smolenski, I. Amelio, A. Popert, T. Chervy, L. Xiaobo, L. Song, K. Barmak, K. Watanabe, T. Taniguchi, D.J. Norris, M. Kroner, and P. A. Murthy, *Nature* **606**, 298 (2022).
 - [20] L. V. Keldysh, *JETP Lett.* **29**, 658 (1979).
 - [21] O.L. Berman and R.Y. Kezarshvili, *Phys. Rev. B* **96**, 094502 (2017).

- [22] P. Cudazzo, I.V. Tokatly, and A. Rubio, Phys. Rev. B **84**, 085406 (2011).
- [23] M. Akhar, G. Anderson, R. Zhao, A. Alruqi, J. E. Mroczkowska, G. Sumanasekera, and J. B. Jasinski, npj 2D Mater. Appl. **1**, 5 (2017).
- [24] J. Qiao, X. Kong, Z. X. Hu, F. Yang, and W. Ji, Nat. Commun. **5**, 4475 (2014).
- [25] S. Larentis, H.C.P. Movva, B. Fallahazad, K. Kim, A. Behroozi, T. Taniguchi, K. Watanabe, S.K. Banerjee, and E. Tutu, Phys. Rev. B **97**, 201407 (2018).
- [26] Y.Zhang, T.-R. Chang, B. Zhou, Y.-T. Cui, H. Yan, Z. Liu, F. Schmitt, J. Lee, R. Moore, Y. Chen, H. Lin, H.-T. Jeng, S.-K. Mo, Z. Hussain, A. Bansil, and Z.-X. Shen, Nature Nanotech **9**, 111 (2014).
- [27] A. N. Rudenko and M. I. Katsnelson, Phys. Rev. B **89**, 201408(R) (2014).
- [28] B. Szafran, Phys. Rev. B **101**, 235313 (2020).
- [29] J. M. Pereira, Jr. and M. I. Katsnelson, Landau levels of single-layer and bilayer phosphorene, Phys. Rev. B **92**, 075437 (2015).
- [30] X. Peng, Q. Wei, and A. Copple, Phys. Rev. B **90**, 085402 (2014).
- [31] B. Sa, Y.-L. Li, Z. Sun, J. Qi, C. Wen, and B. Wu, Nanotechnology **26**, 215205 (2015).